

Kinematic dynamo action in a sphere: Effects of periodic time-dependent flows on solutions with axial dipole symmetry.

Ashley P. Willis and David Gubbins
School of Earth Sciences, University of Leeds, LS2 9JT, UK

April 17, 2024

Abstract

Choosing a simple class of flows, with characteristics that may be present in the Earth's core, we study the ability to generate a magnetic field when the flow is permitted to oscillate periodically in time. The flow characteristics are parameterised by D , representing a differential rotation, M , a meridional circulation, and C , a roll component characterising convective rolls. The dynamo action of all solutions with fixed parameters (steady flows) is known from previous studies. Dynamo action is sensitive to these flow parameters and fails spectacularly for much of the parameter space where magnetic flux is concentrated into small regions, leading to high diffusion. In addition, steady flows generate only steady or regularly reversing oscillatory fields and cannot therefore reproduce irregular geomagnetic-type reversal behaviour. Oscillations of the flow are introduced by varying the flow parameters in time, defining a closed orbit in the space $(D; M)$. When the frequency of the oscillation is small, the net growth rate of the magnetic field over one period approaches the average of the growth rates for steady flows along the orbit. At increased frequency time-dependence appears to smooth out flux concentrations, often enhancing dynamo action. Dynamo action can be impaired, however, when flux concentrations of opposite signs occur close together as smoothing destroys the flux by cancellation. It is possible to produce geomagnetic-type reversals by making the orbit stray into a region where the steady flows generate oscillatory fields. In this case, however, dynamo action was not found to be enhanced by the time-dependence. A novel approach is taken to solving the time-dependent eigenvalue problem, whereby combining Floquet theory with a matrix-free Krylov-subspace method we avoid large memory requirements for storing the matrix required by the standard approach.

Keywords: Kinematic dynamos; Time dependent stability; Geomagnetism; Floquet theory; Eigenvalue problems.

1 Introduction

Unlike the Sun or Jupiter, the Earth's dynamo runs on a tight heat budget and may therefore rely on a significant large-scale component to the flow. In addition to the dominant dipole component of the geomagnetic field, there is some observational evidence to suggest the field contains a persistent non-axisymmetric component (Gubbins and Kelly, 1993). Both may be indicative of a steady component to the underlying core flow. This prompted a kinematic study of dynamo action from a class of large-scale steady candidate core flows (Gubbins et al. (2000a), Gubbins et al. (2000b), Gubbins and Gubbins (2002) hereafter referred to as papers I(III)). Steady flows, particularly if they contain stagnation points, tend to concentrate magnetic flux into small regions with large energy loss due to diffusion. Often, increasing the flow speed to overcome diffusive loss simply results in more concentrated flux and faster decay. On the other hand, chaotic flows appear to make better dynamos, perhaps because the mixing properties of the flow prevents permanent flux concentration and exponential separation of neighbouring particles in the flow lead to stretching of the magnetic field (Brunmell et al., 1998). The dynamo mechanisms of complicated chaotic flows are difficult to understand. We are therefore motivated to first study the effects of simple flows that fluctuate about a steady mean. Although the Earth's dipole has persisted for a long time, secular variation including excursions of the magnetic pole may indicate that fluctuations of the large-scale flow are present in the Earth's core.

Kinematic theory ignores the nonlinearity of back-reaction by the magnetic field on the flow, and considers only the time evolution of the magnetic field as governed by the induction equation

$$\partial_t \mathbf{b} = R_m \mathbf{r} \wedge (\mathbf{u} \wedge \mathbf{b}) + r^2 \mathbf{b} : \quad (1)$$

The induction equation has been non-dimensionalised with the timescale for magnetic diffusion, the length scale d , the radius of the sphere, and in this work the velocity \mathbf{u} is normalised such that the magnetic Reynolds number R_m is unity for a flow of unit kinetic energy. For a given steady flow the induction equation is linear in \mathbf{b} and has eigenfunction solutions of the form $\mathbf{b}(\mathbf{r}; \mathbf{r}; t) = e^{\lambda t} \mathbf{B}(\mathbf{r}; \mathbf{r})$: Dynamo action is established if $\lambda > 0$. This simple test is the major advantage of the kinematic approach. The alternative is to integrate in time the nonlinear problem for both the velocity and magnetic field until one is convinced the magnetic field will not ultimately decay; this is expensive and the results can be uncertain. The advantage remains, however, when the flow varies in time but is periodic; Floquet theory gives an eigenvalue problem for the growth rate.

Backus (1958) was first to show kinematic dynamo action by a time-dependent flow. His dynamo employed periods of stasis while high harmonics in the field decayed, enabling him to establish convergence of the solution.

Time dependence may even lead to dynamo action when no single snapshot of the flow can generate magnetic field on its own. Magnetic fields can grow during an initial transient period under the influence of a subcritical steady flow, the most familiar example being the production of toroidal field from the action of differential rotation on poloidal field. If the induction equation were self-adjoint and its eigenfunctions orthogonal it would be a simple matter to prove that all such transients decay; it is the non-normal property that allows transients to grow. The initial fields which optimise transient growth for flows in a sphere, including one of the flows here, have been studied by Livemore and Jackson (2004). Unfortunately, if the flow is steady the field eventually dies away and only the slowest decaying mode remains. If the flow is permitted to be time dependent, however, once a transient field associated with the initial flow has grown, a change in the flow can encourage further growth. In plane-layer flow it has been shown that by repeatedly switching the orientation of the flow it is possible to take advantage of these transients (Gog et al., 1999), and to find dynamo action where each flow in isolation does not dynamo kinematically.

Another reason to extend the studies to time-dependent flows is that steady flows cannot account for the irregularity of geomagnetic reversals. The induction equation is linear with eigenfunctions that change with time only in magnitude, when $\omega = (\omega) = 0$, or oscillatory solutions that reverse polarity with fixed period $2\pi = (\omega)$. Geomagnetic-type reversals require changes in the flow. Sarson and Jones (1999) described irregular reversals that occurred in simulations with their $2\frac{1}{2}$ -dimensional model. The mechanism could be interpreted kinematically, and reversals were observed to occur when fluctuations in the flow lead to a reduced meridional circulation. More recently Wicht and Olsen (2004) studied reversals in a fully self-consistent but quasi-periodic system. The reversal mechanism they proposed also appeals largely to kinematic principles and appears to reverse with approximately fixed period even when nonlinearity through the Lorentz force is omitted.

The class of steady flows explored in I{III was originally prescribed by Kumar and Roberts (1975) and, with parameters chosen to mimic flows near the limit of Braginsky (1964), was shown to be capable of dynamo action. Dependence of the dynamo on a much wider range of parameter values was later found in I. The Kumar{Roberts flow is confined to the sphere of unit radius, the exterior of which is assumed to be perfectly insulating. Three components of the flow represent a differential rotation, a meridional circulation and a convective overturn,

$$u = \omega_0 t_1^0 + \omega_1 s_2^0 + (\omega_2 s_2^{2c} + \omega_3 s_2^{2s}): \quad (2)$$

Following the nomenclature detailed in I, the ω_i are constrained such that $\omega_2 = \omega_3$ and the kinetic energy of the flow is unity. The flow is parameterised

by $(D; M)$ -space, where $D = D(0)$, $M = M(1)$ and $D_j + M_j = 1$. The parameters D and M are measures of the differential rotation and meridional circulation respectively.

For a steady forcing flow, writing $b(t) = e^{tB}$, where B is independent of t , (1) can be expressed as the eigenvalue problem

$$B = F B; \quad (3)$$

In paper I dynamo action was established for approximately half the $(D; M)$ -space (Fig. 1). Sarson and Gubbins (1996) and III found a number of oscillatory solutions for steady flows in a region which corresponds to the dynamo wave solutions of the ω equations in the Braginsky limit $|D_j| \ll 1$ in a manner such that $1 - D_j = c M_j$ where c is a constant. The oscillatory region was found in I to extend only for a very narrow range in M , shown schematically in Fig. 1. The majority of solutions are steady. Given the narrow range for M , it is apparent that only a small degree of meridional circulation is required to stabilise the field to steady solutions. On the other hand, the existence of oscillatory solutions for low M appears to be a fairly robust feature as the range in D for which they exist is large, and extends well beyond the limit of Braginsky.

In this work, the exploration above is extended to the dynamo action of flows with $D = D(t)$ and $M = M(t)$ periodic in time, with a given period T . The induction equation (1) can be written as

$$\partial_t b = F(t) b; \quad (4)$$

with periodic forcing $F(T + t) = F(t)$. It follows from Floquet's theorem (see x2) that solutions may be written in the form $b(T + t) = e^{\lambda T} b(t)$ where the real part of λ is the net growth rate over one period. Setting $b(t) = e^{\lambda t} B(t)$, so that $B(T + t) = B(t)$, substitution into (4) defines the eigenvalue problem for B ,

$$\lambda B = (F - \partial_t) B; \quad (5)$$

The critical magnetic Reynolds number for which the field is marginally stable, $\lambda = 0$, is denoted R_m^c .

Both the steady and non-steady eigenvalue problems (3) and (5) permit solutions for four linearly independent spatial symmetries, axial dipole, axial quadrupole, equatorial dipole and equatorial quadrupole. Symmetry selection in the steady case was studied in II. Here only the geophysically interesting axial dipole symmetry will be considered.

2 Numerical method

Steady flows have been studied using extensions of the method first developed by Bullard and Gellman (1954). Toroidal and poloidal potentials for

the magnetic field are expanded in spherical harmonics, with truncation at degree L . A finite difference scheme is applied on N_r points in the radial dimension leading to the discretised eigenvalue problem

$$B = EB : \quad (6)$$

The matrix E has dimensions $N_r N_h \times N_r N_h$, where after symmetry considerations the number of harmonics $N_h \sim \frac{1}{2}L^2$. As the finite difference scheme only connects neighbouring points, E is block banded where each block has size $N_h \times N_h$. Eigenvectors are then calculated by either by inverse iteration or by the Implicitly Restarted Arnoldi Method (IRAM) on the inverse. Due to the performance of both methods with respect to the distribution of the eigenvalues, both operate on the inverse and require the (banded) LU factorisation of E . Memory requirements scale like several times $N_h^2 N_r$, depending on the stencil size of the finite difference approximation. Solutions have generally been calculated with second order differences, and L not much larger than twenty. The storage requirement for the large matrix is the limiting factor for the calculation.

For the time-dependent eigenvalue problem (5) with the same spatial representation, applying a Fourier expansion in time introduces at least another factor N_t to the storage requirements. This can be minimised by permitting only sinusoidal forcings, but due to the structure of the matrix memory requirements are prohibitive with respect to calculation of the LU factorisation (a few times $N_h^2 N_r^2 N_t$). Storage is a significant difficulty in multiplying by the inverse or in calculating the inverse of a suitable preconditioner for the time-dependent problem.

Instead we have adopted a method that does not require storage of the matrix, which we call the matrix-free Krylov subspace method. It is an adaptation of a method used to find steady solutions of the Navier-Stokes equations by Edwards et al. (1994). Periodicity of the flow is incorporated in the following manner (Verhulst, 1996). Writing the discrete form of (4) as

$$\partial_t b = F(t)b; \quad (7)$$

the matrix $G(t)$ satisfying $\partial_t G(t) = F(t)G(t)$; with $G(0) = I$; is the fundamental matrix of the system (7). Evolution of a starting solution is then given by

$$b(t) = G(t)b(0); \quad (8)$$

For any T -periodic $F(t)$, there exist matrices $P(t)$ and E such that the fundamental matrix can be written

$$G(t) = P(t)e^{Et}; \quad (9)$$

where E is independent of t and $P(t)$ is T -periodic (Floquet's theorem). It follows immediately that the change in the solution over one period is given

by

$$b(T) = G(T)b(0); \quad G(T) = e^{E T} = A: \quad (10)$$

The stability of solutions to (7) is determined by the eigenvalues of the constant matrix A . If $b(0)$ is an eigenvector of A with eigenvalue $\lambda = e^{-1T}$, we find that $b(T+t) = e^{-1T} b(t)$ for any t . The real part of the Floquet exponents λ_1 correspond to growth rates of the solutions. Although A is unknown, from (8) we see that the effect of multiplying by A is equivalent to the result of time stepping through one period. Therefore we do not have to calculate and store A explicitly. Note that for a steady forcing F , the period T can be chosen arbitrarily.

The eigenvalue problem for A is well suited to the Arnoldi process (Arnoldi, 1951), which tends to pick out eigenvalues isolated in the complex plane. The many decaying modes have clustered about the origin, marginal modes correspond to λ_j close to unity. At each iteration we add to the Krylov-subspace given by $\text{span}\{b; Ab; \dots; A^{k-1}b\}$ which we hope contains our solutions. In exact arithmetic the k^{th} Krylov subspace is equivalent to $\text{span}\{b_1; \dots; b_k\}$ where the basis vectors b_k are obtained from the Arnoldi method. Numerically the latter set is better suited to span the space. The Arnoldi process is summarised as follows: (1) Take a suitable normalised initial basis vector $b_1 = b/\|b\|_2$. (2) At the k^{th} iteration evaluate (time step) $\tilde{b}_{k+1} = A b_k$. (3) The result \tilde{b}_{k+1} is then orthogonalised against previous vectors in the basis by the modified Gram-Schmidt method:

$$h_{jk} = \tilde{b}_{k+1}^T b_j; \quad \tilde{b}_{k+1} = \tilde{b}_{k+1} - \sum_{j=1}^k h_{jk} b_j; \quad j = 1, \dots, k:$$

(4) Setting $h_{k+1,k} = \|\tilde{b}_{k+1}\|_2$, the process continues from (2) with the next basis vector $b_{k+1} = \tilde{b}_{k+1}/h_{k+1,k}$. Construct $Q_k = [b_1; \dots; b_k]$ and $H_k = [h_{jm}]_{j,m=1}^k$. From steps (3) and (4) we expect $h_{k+1,k} \neq 0$. In this case, looking carefully at the steps above, the results of the Arnoldi process can be written $AQ_k = Q_k H_k$. Multiplying on the right by eigenvectors x of H_k we find that they are related to those of A by $b = Q_k x$. For non-zero $h_{k+1,k}$ eigenvectors have residual $\|kA b - b\|_2 = \|h_{k+1,k} \tilde{b}_k\|_2$ where x_k is the last element of the k -vector x . Thus, at each iteration eigenvalues of H_k are approximate eigenvalues of A .

In practice the residual $\|h_{k+1,k} \tilde{b}_k\|_2$ tends to overestimate the error, and in our calculations the Arnoldi process is stopped when the largest eigenvalues of H_k are sufficiently converged. The number of iterations required is typically of order 100 or less, and so the eigenvalues of the small matrix H_k can be cheaply calculated by the QR algorithm. The memory required to store the basis vectors scales like $N_h N_r k$. It is possible to restart the Arnoldi process with a more suitable starting vector obtained from the process so far, but without completely restarting the new process from scratch. This implicit restarting allows further reduction of memory requirements by reducing the number of basis vectors at each restart (Lehoucq et al., 1998).

With k small, restarting was not found to be necessary, however. The stencil of the finite difference scheme does not explicitly affect the storage requirements. Basis vectors were therefore time-stepped with a fourth order finite difference scheme. Time-stepping was performed with the benchmarked code of Gibbons, Jones and Zhang (Christensen et al., 2001).

Another advantage of the matrix-free method is that, given a time-stepping code, only a few extra lines of code are required to incorporate the Arnoldi process, therefore leaving significantly less room for error. The code was verified by comparison with the matrix method used in I{III} for the steady problem, adjustments for the periodic case in our matrix-free method are minimal. Table 1 (a) shows the leading two eigenvalues for the of the steady Kumar(Roberts flow, $(D;M) = (0.98354915; 0.0001632689)$, at $R_m = 1000$ calculated using the method in I{III}. Table 1 (b) shows the same eigenvalues calculated using our method. The higher order radial differences used in the time-stepping code leads to more rapid convergence with N_r . Table 1 (c) shows that incorporating the Arnoldi method accelerates convergence relative to time-stepping alone (and calculation of more than one eigenvalue is possible). The same starting vector was used for both calculations. The period T can be chosen arbitrarily for the steady flow case, but if chosen too small more iterations are required and therefore more basis vectors must be stored. For these calculations we set $T = 0.001$.

As the structure of the eigenfunctions varies with D and M , so does the convergence with N_r and L . For most of the following analysis a radial resolution of $N_r = 50$ and a spectral truncation of $L = 18$ was adopted. Checks at higher resolutions were calculated where growth rates were found to vary rapidly with the parameters.

3 Results

Periodic flows are defined by a closed orbit in $(D;M)$ -space. We restrict ourselves to simple sinusoidal variations in time with a single frequency ω :

$$\begin{aligned} D(t) &= D_0 + A_D \cos(\omega t); \\ M(t) &= M_0 + A_M \sin(\omega t); \end{aligned} \tag{11}$$

It is the aim of this section to assess how the amplitude of variations A_D, A_M and frequency ω affect the growth rates and therefore the dynamo action.

3.1 Magnetic growth rates for time-varying flows

Figure 2 shows growth rates for different amplitudes of variations about the point $(D_0; M_0) = (0.25; 0.14)$, marked A in Fig. 1, which lies on a line of minimum R_m extending from the Braginsky limit point $(1; 0)$ (see I, Table 5). The majority of neighbouring points have lower growth rates for

the given value of $R_m = 87$. Figure 2 shows that the effect of oscillations of the flow on the growth rates is more pronounced with increased oscillation amplitude.

For a steady flow, given any small real number $\epsilon > 0$ there exists a finite time t such that transients are reduced so that $|j_1(t) - j| < \epsilon$, where j is the growth rate corresponding to the steady flow at each point on the orbit, and $j_1(t)$ is the growth rate of an arbitrary initial field as it adjusts to the flow. Provided that growth rates are piecewise continuous (for example $j_1(t)$ could be discontinuous but periodic, see Backus 1958), a frequency ω can always be selected low enough such that net growth rate over the cycle is close to the mean of those on the orbit. The limit $\lim_{\omega \rightarrow 0} j_1(\omega) = j$ is observed in the numerical calculations. What is more interesting, however, is that with finite ω the dynamo can do much better than this mean, $j_1(\omega) > j$, as seen in most figures for the growth rate. Figure 3 shows that the effect increases with R_m and that the peak occurs at a frequency ω that increases in proportion to R_m .

Meridional sections of the magnetic field for this flow are plotted in Figure 4. The two times correspond closely to the points on the orbit which have the maximum (upper row) and minimum growth rates for steady flows ($\omega = 0$). The structure of these eigenfunctions is similar; regions of B are generally well separated in space. The dissipation for these fields is larger for the lower panel where fields of opposite sign are squeezed towards the equator. For non-zero ω the location of the flux changes over the cycle, and at $\log \omega = 2.6$ the field represents a smoothed version of the two eigenfunctions. Fewer small-scale features are present and the flow performs well as a dynamo (see Figure 3). At $R_m = 150$ the peak frequency for j_1 is $\log \omega = 2.6$; taking $T = (d^2/\nu)$ as an approximate timescale for diffusion, if $d = 8$ is an approximate length scale for the small-scale features of the eigenfunctions, we find that the timescale for diffusion and for the peak flow oscillation coincide. The magnetic field is then smoothed effectively. Above this frequency the growth rate decreases again as the field is unable to respond to rapid changes in the flow. Spatial smoothing is lost and the field is close to steady state plots at the two times for $\log \omega = 2.9$ are almost identical. The field responds as though to a steady flow, retaining the stronger (smaller-scale) features from each eigenfunction.

Figure 5 shows growth rates for an orbit about the point $(0.5; 0.15)$, marked B in Figure 1, which lies on the lower boundary of the region of successful steady dynamos. D remains constant and M varies to carry the flow outside the dynamo region. The time-dependent flow produces a positive effect on the growth rate. The spatial structure of the eigenvectors on this orbit is similar to that of the previous point considered, with well separated regions of positive and negative azimuthal field. For $R_m = 150$ there is dynamo action only for frequencies $\log \omega = 2.6$, and the average growth rate around the orbit is negative.

We now describe a case where meridional circulation is greater than differential rotation, $(D;M) = (0.10; 0.45)$, marked C in Fig. 1. This point is close to where the critical magnetic Reynolds number for steady flows is at a global minimum. Once again time dependence of the flow enhances the growth rate, Fig. 6. A small rise can be seen in the growth rate, although less significant relative to the increase associated with an increase in the magnetic Reynolds number. Being close to the point where R_m^c is a minimum, the fields are already relatively large scale and the smoothing effect of oscillations therefore has a smaller effect on the growth rate.

Growth of the time-dependent solutions is not always found to be better than the mean of the growth rates on the orbit. Figure 7 shows the case $(D;M) = (0.50; 0.11)$, marked D in Fig. 1, where oscillations in the flow are initially damaging to the dynamo. If the oscillations are sufficiently rapid, however, the dynamo is again able to perform better. Meridional sections are shown in Fig. 8. The regions of strongest flux are located very close together on the equator. Over the cycle radial shifts of the clover-leaf pattern of flux causes considerable overlap of opposite signs. This occurs mostly towards the outer edge of the equatorial region. As the flow oscillates, in the lower plot for $\log \tau = 2.13$ it can be seen that there is cancellation of flux in the outer region. Some flux remains at the other regions where the signs for the two eigenfunctions do correlate. This cancellation of fluxes over the cycle leads to reduced growth rates. When the oscillation is much faster, however, the dynamo does not have time to generate flux of opposing sign. The field is more steady for $\log \tau = 2.60$ and has a larger growth rate.

The radial field in the above has little structure of interest. It is concentrated mainly on the axis with opposite sign in each hemisphere (see I, Fig. 9a,b). The structure does not change appreciably over the cycles. In strength, however, it is observed to wax and wane.

3.2 Dynamo wave solutions

Meridional circulation has been seen to play a key part in reversals. Sarson and Jones (1999) have studied a system in which irregular reversals are linked to a drop in meridional circulation, leading to a preference for oscillatory fields. Wicht and Olsen (2004) have recently studied a reversal mechanism that involves an advection of reversed flux by a large-scale S1 flow. Reversals occur quasi-periodically in their model. This behaviour may be related to the dynamo wave solutions obtained in III. The oscillation has the form of a dynamo wave in which flux migrates along the longitudes defined by the downwellings of the convective parts of the flow, which could partially explain the observed tendency for virtual geomagnetic poles to track around the Pacific during polarity transition (Gubbins and Sarson, 1994). The steady flow model can only oscillate periodically, but we can construct a more geophysically realistic reversal by choosing a time-dependent flow that

traces an orbit in $(D;M)$ -space that strays into the dynamo wave region, depicted by the line E in Fig. 1, for a fraction f of its period. The field behaviour will depend on the frequency of the dynamo wave, ω_D and the time spent by the flow in the oscillatory regime. If $\omega_D \gg \omega$ the flow will only spend a brief time in the oscillatory regime and we expect only a minor change in the magnetic field. If $\omega_D \approx \omega$ the flow spends a long time in the oscillatory regime and we expect the field to oscillate several times before becoming steady again. The interesting case is when $\omega_D \approx \omega/2$, when the field may only have time to oscillate for one or a half cycle, producing an excursion or a reversal respectively.

We now explore reversal behaviour using periodic flows. The structure of the eigenfunctions for steady flows changes appreciably as M crosses zero. It was seen in the previous section that, where this is the case, fluctuations are not necessarily good for the dynamo. Instead, an orbit is chosen to enter the oscillatory range from the negative side. Consider the flow defined by fixed $D = 0.7$ and M varying sinusoidally between -0.0140 and 0.0020 (E in Fig. 1). This orbit spends approximately one third of the time within the band of oscillatory solutions reported in III, which lies between $M = -0.0057$ and 0.0010 . The dynamo wave frequency for steady flows increases with R_m and appears to saturate at about $\omega_D = 17$ (see III, Figs 2,3); it appears to be limited by the diffusion time. Here, ω for the time-dependent flow must be chosen comparable with this frequency to give a single reversal, a value which is too low to assist the dynamo action significantly.

Figure 9 shows the growth rate for the time dependent flows as a function of frequency ω . At $R_m = 700$, $\omega_D = 17$ is approximately 10 for steady flows in the oscillatory range. Reversing solutions may be expected for $\omega \approx \omega_D/3$, or equivalently $\omega \approx 5.7$, as the time in the oscillatory range is approximately one third of the cycle. Reversing solutions (dashed curve) are observed for ω larger than the dynamo wave frequency, although growth rates fall quickly when the period of the flow oscillation is too short to be compatible with the period of the oscillatory solution. If the time within the oscillatory region leads to only a half-complete reversal, the field exiting the region bears little resemblance to the entering field, which is much like the eigenfunction for these low ω , and therefore leads to reduced growth rates. For greater ω the field does not spend sufficient time within the oscillatory region to reverse (solid curve) and at higher ω the growth rates are increased. The magnetic energy for a typical reversing solution is plotted in Fig. 10, showing a drop as the solution passes through the oscillatory region where the reversal occurs. It is possible to vary M so that f is less than a third. However, for the reversing solution in Fig. 10, the smooth growth rate curve, while outside the oscillatory region, indicates the field quickly becomes independent of the period within the oscillatory region, apart from in sign, due to the slow period of the flow oscillation.

The reversal sequence for B_r at the surface is shown in Fig. 11. Patches of reversed flux appear at low latitudes, strengthen and migrate polewards replacing the flux at high latitudes. The reversal looks very similar to that reported by Gubbins and Sarson (1994) who found the pole paths during the reversal correlate well with the longitudes of these flux patches, located 180° apart. If the frequency of the oscillation is too high the field is simply disrupted by the short period in the oscillatory region, as seen in the energy in Fig. 10. This may lead to the type behaviour seen in geomagnetic excursions. Figure 12 shows that reversed patches emerge but have insufficient time to migrate polewards before dissipating. They still weaken the dipole, however.

4 Conclusions

We have devised a new matrix-free Krylov subspace approach to solving the time-dependent stability problem that is most effective in exploring kinematic dynamo action of periodic flows. It is computationally efficient, uses far less storage than conventional methods, and requires rather little new coding once time-step and eigenvalue routines are available.

Time variation of the flow can sometimes, but not always, enhance dynamo action. At low frequency the growth rate of the time dependent flow approaches the average growth rate for the steady flows along the orbit. At moderate frequency the time dependent flow can smooth out any concentrations of magnetic flux generated by the component steady flows. This can produce enhanced dynamo action (higher growth rate than the average) if the flux concentrations are isolated and of one sign. Dynamo action is possible at certain frequencies even when the average growth rate for steady flows around the cycle is negative and the cycle contains mainly steady flows that do not generate magnetic field. The growth rate appears to be capped by the highest growth rate of any steady flow on the cycle. At high frequency the magnetic field does not have time to adjust to time changes in the flow and becomes almost stationary.

Time variation does not always enhance dynamo action. When the generated field has flux concentrations of different signs close together, the smoothing effect tends to destroy flux. The dynamo enhancement for these large scale flows is not as dramatic as those reported by Gog et al. (1999). Flows with similar eigenfunctions tend to have similar growth rates at the same R_m , limiting the effect of the time variation. Where the eigenfunction changes dramatically dynamo action is usually impaired unless the period of the flow is short compared with the diffusion time.

Solutions have been found that reverse when M is low and are associated with the steady-flow oscillatory solutions found in II. This result is in common with the reversals studied by Sarson and Jones (1999), which

occur irregularly due to a drop in meridional circulation. Although flows in their calculations are also predominantly equatorial antisymmetric, a small but increased flow across the equator is observed during a reversal. It is unclear that this results in sufficient advection of flux to influence their reversal mechanism. A large circulation exterior to the tangent cylinder is required in the reversal mechanism studied by Wicht and Olsen (2004). It is needed to transport reversed flux originating from plumes that protrude the tangent cylinder. However, it is difficult to decipher what perturbation would play in their model, and in particular to what degree this would affect the quasi-regularity of their reversals. We have shown that for a reversal to occur the drop in M must persist long enough for the field to reverse, which for this class of flows this is approximately a tenth of a diffusion time, or approximately the dipole decay time. A significant drop in magnetic energy is observed during the reversal. This arises because of the change in eigenfunction between the steady and oscillatory modes of the steady solutions.

Acknowledgements

This work was supported by NERC grant GR3/12825. We thank Johannes Wicht and an anonymous referee for useful comments, and Dr SJ Gibbons for advice on using his time-step code.

References

- Arnoldi, W. E. (1951). The principle of minimized iterations in the solution of the matrix eigenvalue problem. *Q. J. Appl. Math.* 9, 17{29.
- Backus, G. (1958). A class of self-sustaining dissipative spherical dynamo. *Annals of Physics* 4, 372{447.
- Braginsky, S. I. (1964). Kinematic models of the Earth's hydrodynamic dynamo. *Geomagnetism and Aeronomy* 4, 572{583.
- Brummell, N. H., C. F., and S. M. Tobias (1998). Linear and nonlinear dynamo action. *Physics Letters* 249, 437{442.
- Bullard, G. E. and H. Gellman (1954). Homogeneous dynamo and terrestrial magnetism. *Phil. Trans. R. Soc. Lond.* 250, 543{585.
- Christensen, U. R., J. Aubert, P. Cardin, E. Dormy, S. Gibbons, G. A. Glatzmaier, E. Grote, Y. Honkura, C. Jones, M. Kono, M. Matsushima, A. Sakuraba, F. Takahashi, A. Tilgner, J. Wicht, and K. Zhang (2001). A numerical dynamo benchmark. *Phys. Earth Planet. Int.* 128, 25{34.
- Edwards, W. S., L. S. Tuckerman, R. A. Friesner, and D. C. Sorensen (1994). Krylov methods for the incompressible Navier-Stokes equations. *J. Comput. Phys.* 110, 82{102.

- Gog, J.R., I.Oprea, M.R.E.Proctor, and A.M.Rucklidge (1999). Destabilisation by noise of transverse perturbations to hetroclinic cycles: a simple model and an example from dynamo theory. *Proc. R. Soc. Lond.* 455, 4205{4222.
- Gubbins, D., C.N.Barber, S.Gibbons, and J.J.Love (2000a). Kinematic dynamo action in a sphere. I - Effects of differential rotation and meridional circulation on solutions with axial dipole symmetry. *Proc. R. Soc. Lond.* 456, 1333{1353.
- Gubbins, D., C.N.Barber, S.Gibbons, and J.J.Love (2000b). Kinematic dynamo action in a sphere. II - Symmetry selection. *Proc. R. Soc. Lond.* 456, 1669{1683.
- Gubbins, D. and S.Gibbons (2002). Three-dimensional dynamo waves in a sphere. *Geophys. Astrophys. Fluid Dynamics* 96, 481{498.
- Gubbins, D. and P.Kelly (1993). Persistent patterns in the geomagnetic field over the past 2.5M yr. *Nature* 365, 829{832.
- Gubbins, D. and G.R.Sarson (1994). Geomagnetic field morphologies from a kinematic dynamo model. *Nature* 368, 51{55.
- Kumar, S. and P.H.Roberts (1975). A three-dimensional kinematic dynamo. *Proc. R. Soc. Lond.* 244, 235{258.
- Lehoucq, R.B., D.C.Sorensen, and C.Yang (1998). *Arpack users guide: solution of large scale eigenvalue problems by implicitly restarted Arnoldi methods.* Philadelphia, PA : SIAM .
- Livemore, P.W. and A.Jackson (2004). On magnetic energy instability in spherical stationary flows. *Proc. R. Soc. Lond.* 460, 1453{1476.
- Sarson, G.R. and D.Gubbins (1996). Three-dimensional kinematic dynamos dominated by strong differential rotation. *J. Fluid Mech.* 306, 223{265.
- Sarson, G.R. and C.A.Jones (1999). A convection driven geodynamo reversal model. *Phys. Earth Planet. Int.* 111, 3{20.
- Verhulst, F. (1996). *Nonlinear differential equations and dynamical systems.* Springer, Berlin.
- Wicht, J. and P.Olsen (2004). A detailed study of the polarity reversal mechanism in a numerical dynamo model. *Geochem. Geophys. Geosyst.* 5, No. 3, Q03H10.

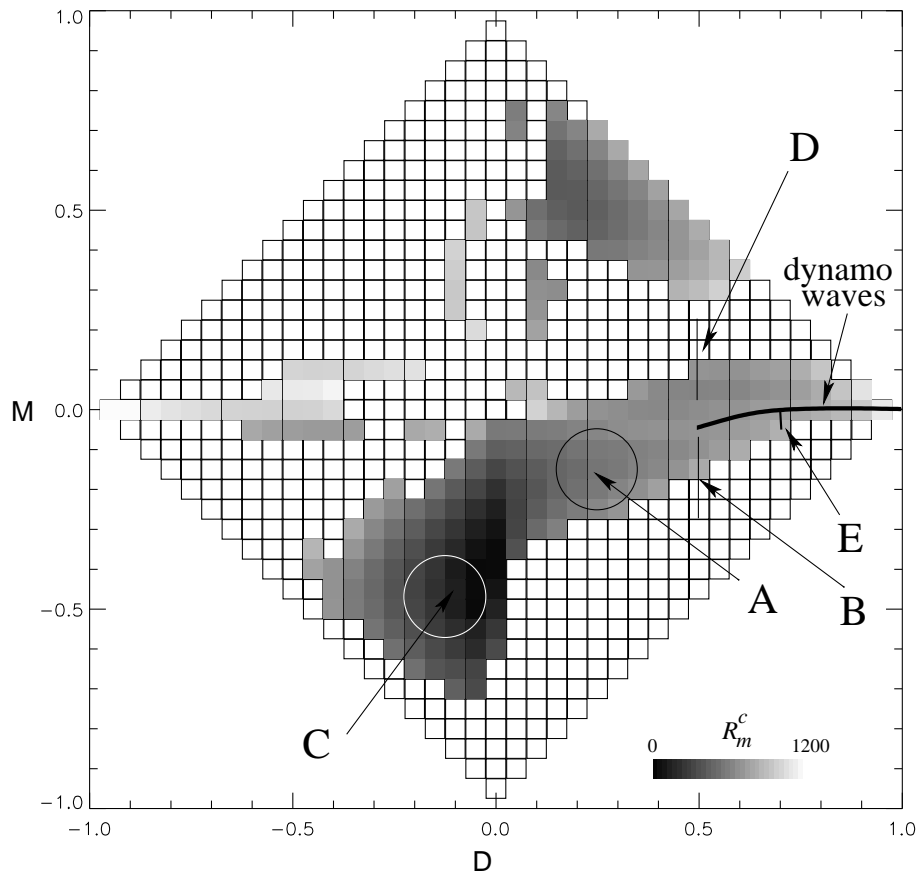


Figure 1: Regions of dynamo solutions for steady flows and axial-dipole symmetry for the flow parameterisation: D , differential rotation; M meridional circulation. The thick line running into the right hand apex contains oscillatory solutions related to the dynamo waves of the Braginsky limit. Other lines and circles describe periodic flows mentioned in the text.

(a)				(c)		
	$N_r = 50$	100	150	k	λ_1	(t_k)
$L = 8$	0.86410	0.95152	0.95593	10	-22.29762	81.56889
12	0.86705	0.95388	0.95826	20	-6.12153	27.14633
16	0.86717	0.95400	0.95838	30	0.79446	4.61364
8	-36.137	-36.406	-36.420	40	2.24163	-3.58609
12	-35.717	-35.959	-35.971	50	0.98918	-3.14851
16	-35.704	-35.954	-35.958	60	0.91102	0.43870
				70	0.95688	3.19484
				80	0.95722	4.12172
(b)				90	0.95721	3.87464
	$N_r = 25$	50	75	100	0.95721	3.19592
$L = 8$	0.98156	0.94976	0.95479	120		1.91438
12	0.99434	0.95211	0.95709	150		1.09479
16	0.99446	0.95223	0.95721	200		0.98221
8	-36.239	-36.452	-36.431	250		0.96445
12	-35.788	-36.005	-35.984	300		0.95774
16	-35.776	-35.991	-35.971	400		0.95735
				500		0.95733

Table 1: Comparison of computed growth rates for the K (Row, (0.9834915; 0.0001632689), at $R_m = 1000$; (a) leading two eigenvalues computed using the matrix and its LU factorisation; (b) eigenvalues calculated by the matrix-free method; (c) comparison with simple time stepping, $T = 0.001$, $t_k = kT$ and $N_r = 75$, $L = 16$.

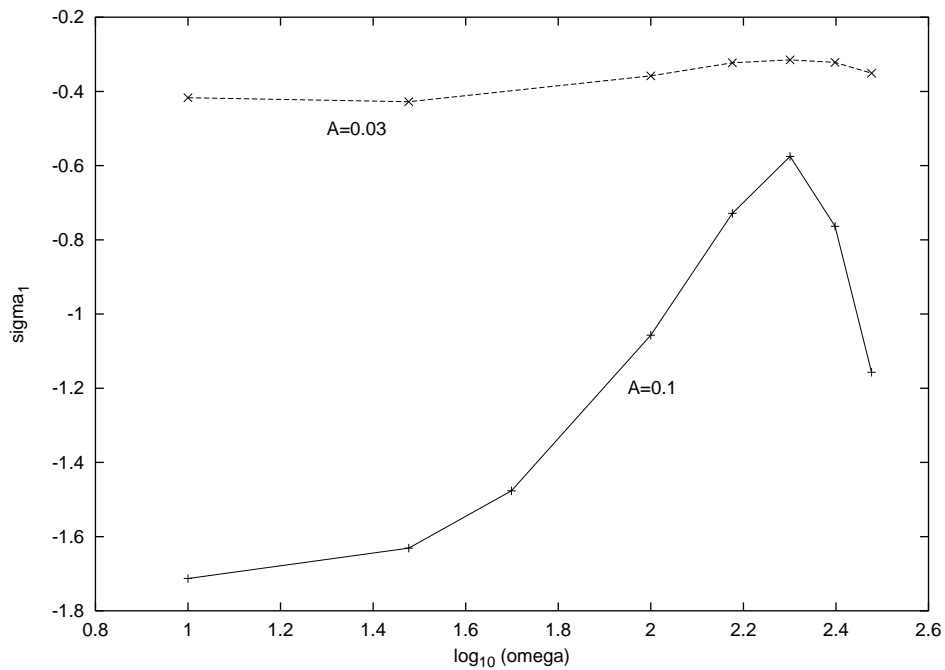


Figure 2: Growth rates σ_1 vs. ω for different amplitudes $A_D = A_M = A$ about the point $(0.25; 0.14)$.

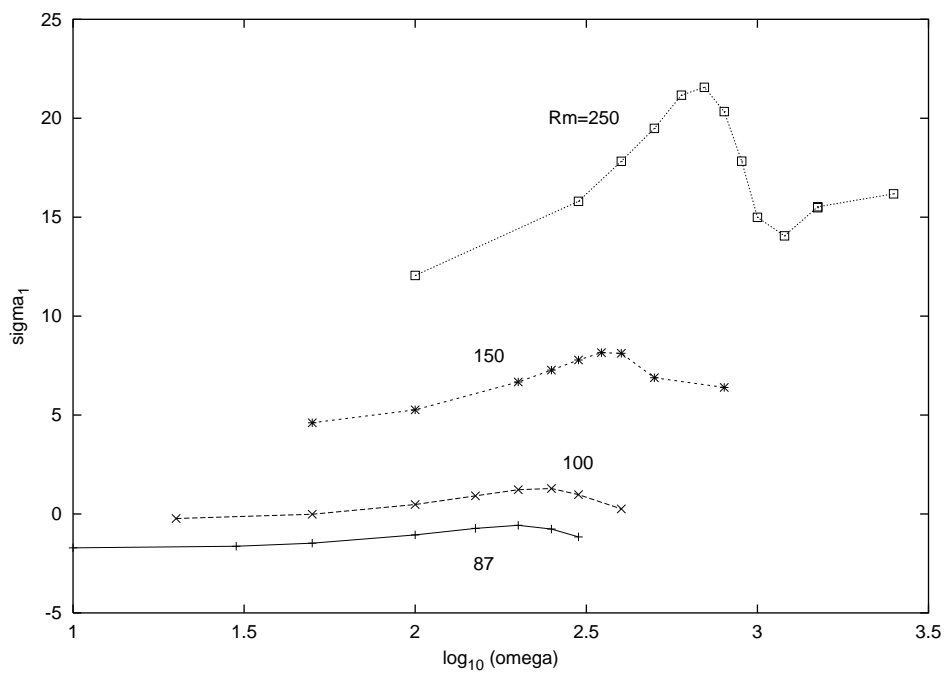


Figure 3: As Fig. 2 for various R_m ; $A_D = A_M = 0.1$, A in Fig. 1.

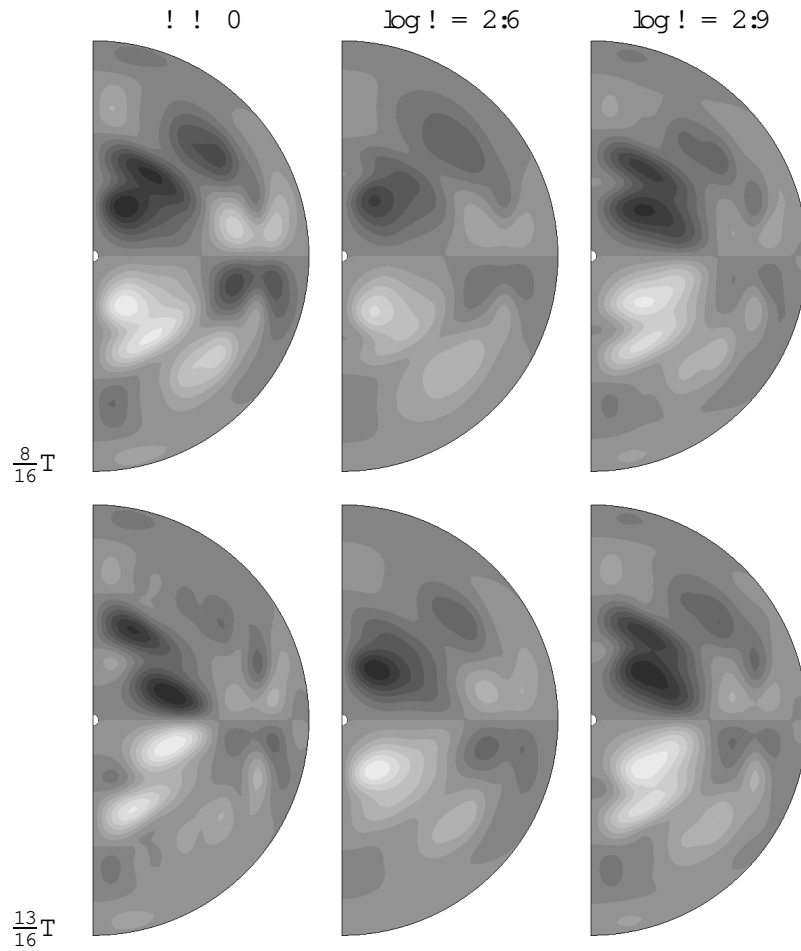


Figure 4: Meridional sections, $B_z = 2$; $R_m = 150$, $(D; M) = (0.25; 0.14)$, $A_D = A_M = 0.1$. Eigenfunctions were calculated for steady flows at the appropriate point and are plotted with independent contour values; for $t \neq 0$, contours are plotted for the same values at different times. At $\log t = 2.6$ the field structure looks smooth. At $\log t = 2.9$ the flow changes too quickly for the field to respond and the field is almost steady.

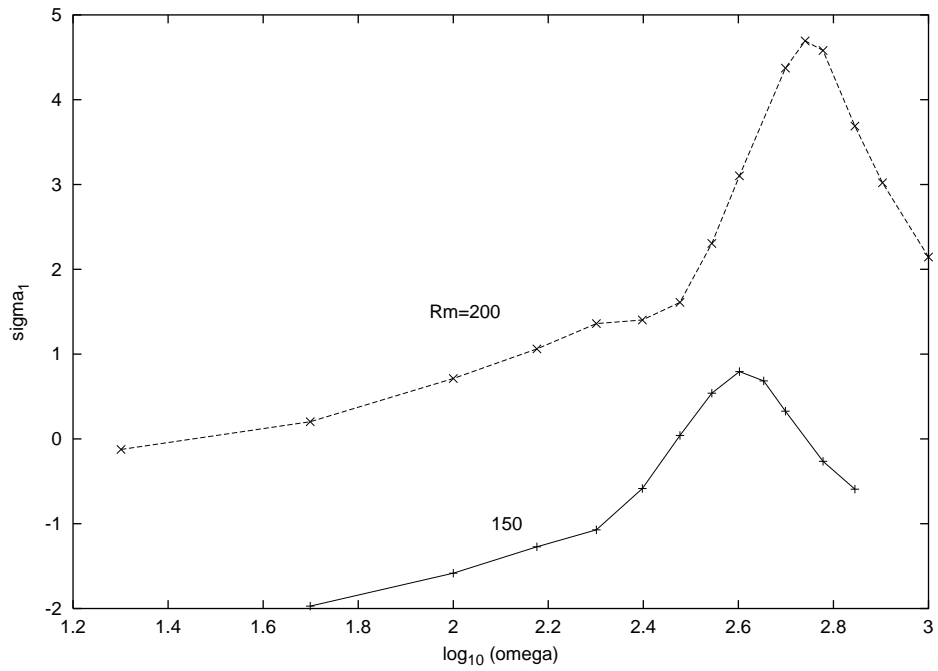


Figure 5: Growth rates σ_1 vs. $\log_{10}(\omega)$ for an orbit about the point $(0.5; 0.15)$; $A_D = 0, A_M = 0.1$ (Fig. 1, B).

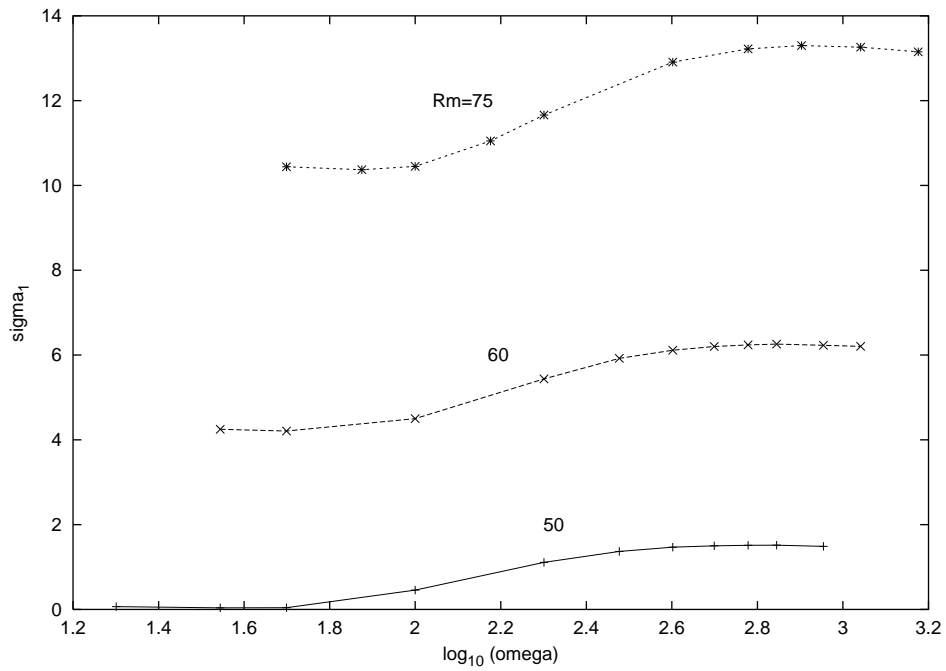


Figure 6: Rising growth rates for an orbit about $(0.1; 0.45)$; $A_D = A_M = 0.1$ (Fig. 1, C).

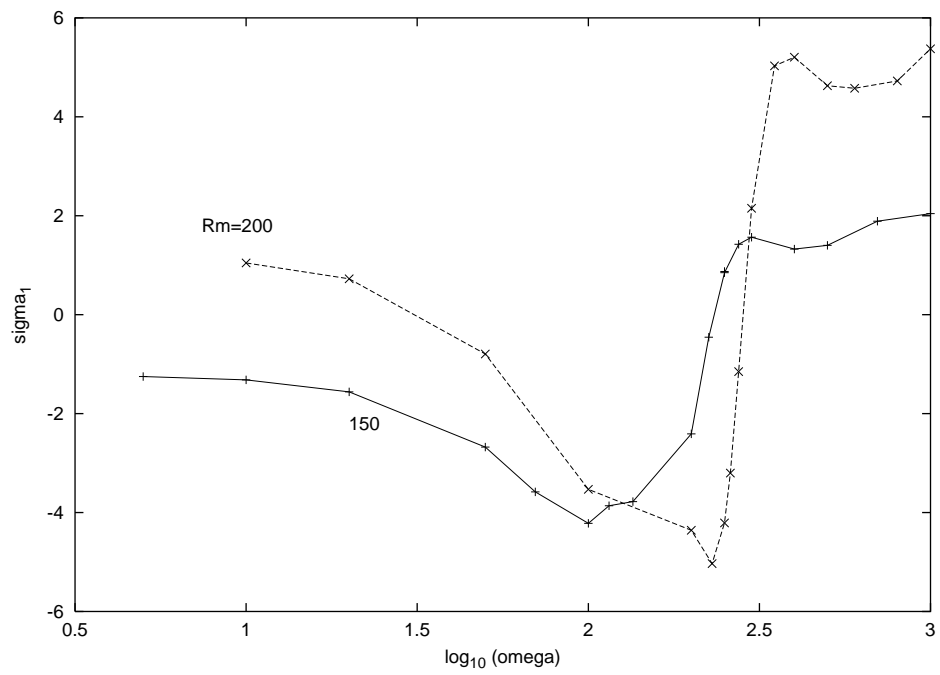


Figure 7: Growth rates for increasing ℓ about the point $(0.5; 0.11)$; $A_D = 0$, $A_M = 0.1$ (Fig. 1, D).

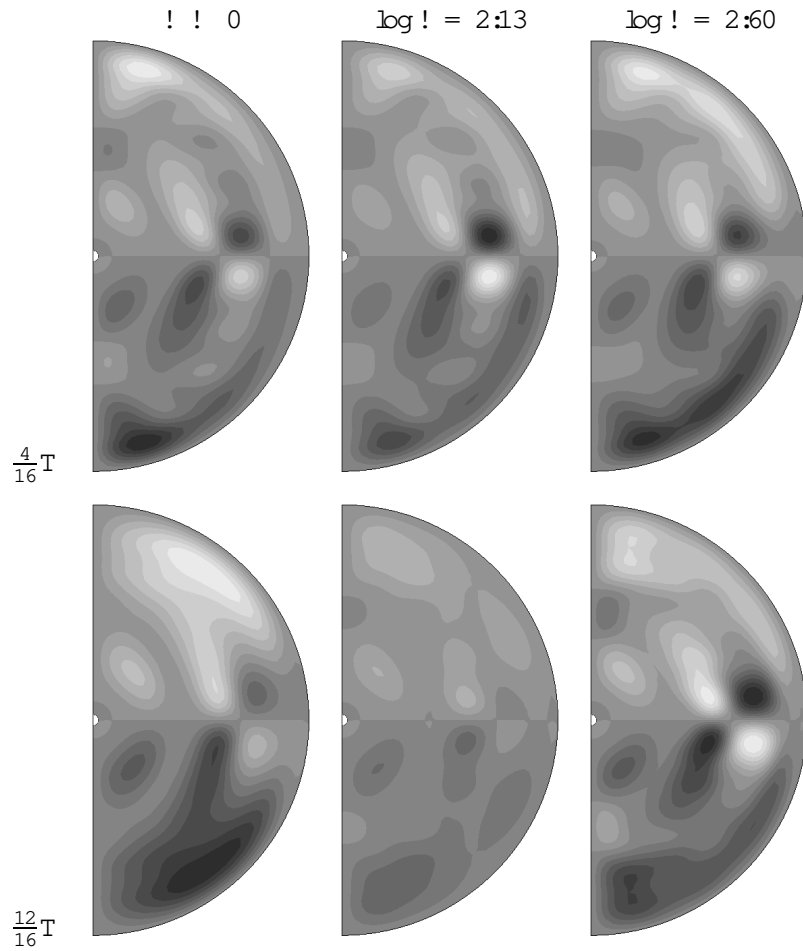


Figure 8: Meridional sections, $B_{\theta} = 0$; $R_m = 150$, $(D; M) = (0.5; 0.11)$, $A_D = 0$, $A_M = 0.1$. The times $t = \frac{4}{16}T$ and $\frac{12}{16}T$ correspond to maximum and minimum $M(t)$ respectively. There is a radial shift of the 'clover' pattern near the equator for the eigenfunctions ($l = 0$). Close proximity of opposing flux leads to cancellation seen towards the outer boundary, lower panel with $\log l = 2.13$. At $\log l = 2.60$ the field is more steady.

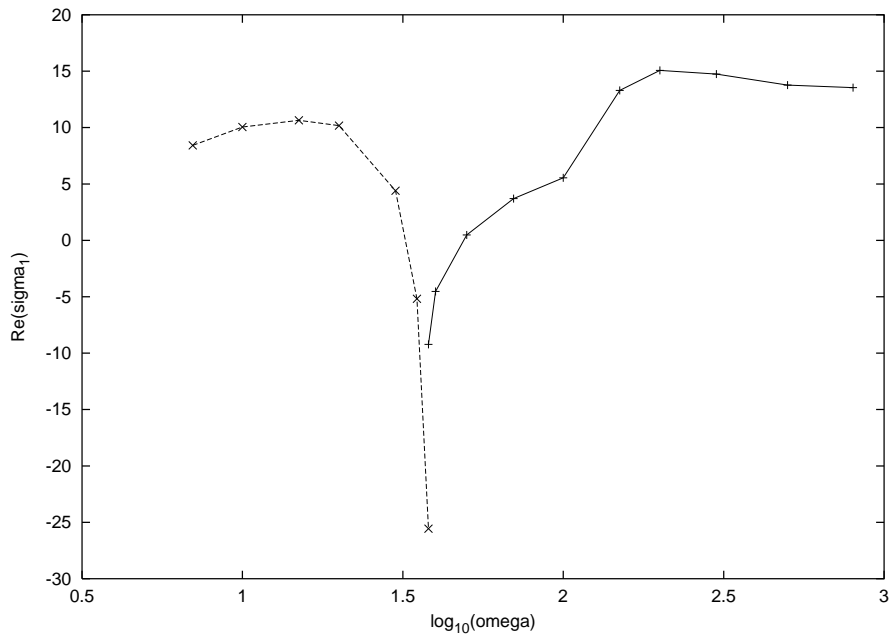


Figure 9: $\langle \sigma_1 \rangle$, $R_m = 700$ at $(D; M) = (0.7; 0.008)$, $A_D = 0$, $A_M = 0.006$ (Fig. 1, E). For the dashed curve $\langle \sigma_1 \rangle = -2$.

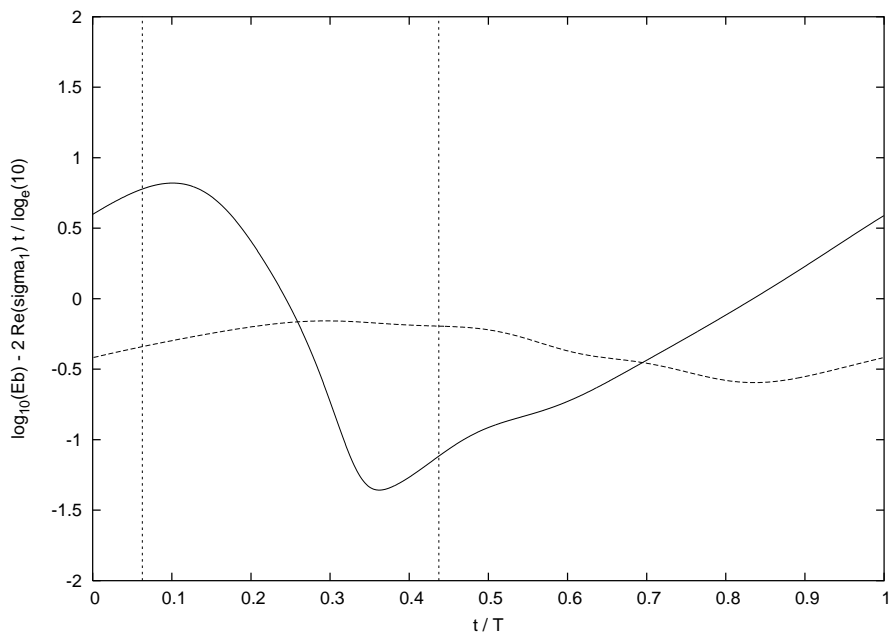


Figure 10: Magnetic energy (minus net growth) for parameters as Fig. 9. Reversing solution $\log \omega = 1.30$ (solid); failed reversal $\log \omega = 2.00$ (dashed). Vertical bars represent the period in the oscillatory regime.

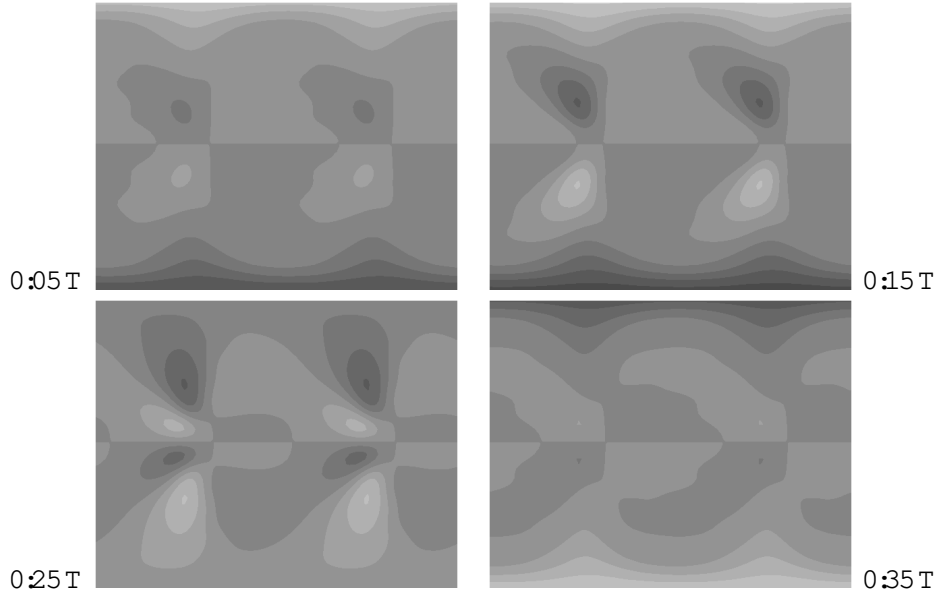


Figure 11: B_r at the surface during the reversal in Fig. 10. Patches of reversed flux near the equator migrate polewards, replacing the flux at high latitudes with reversed field.

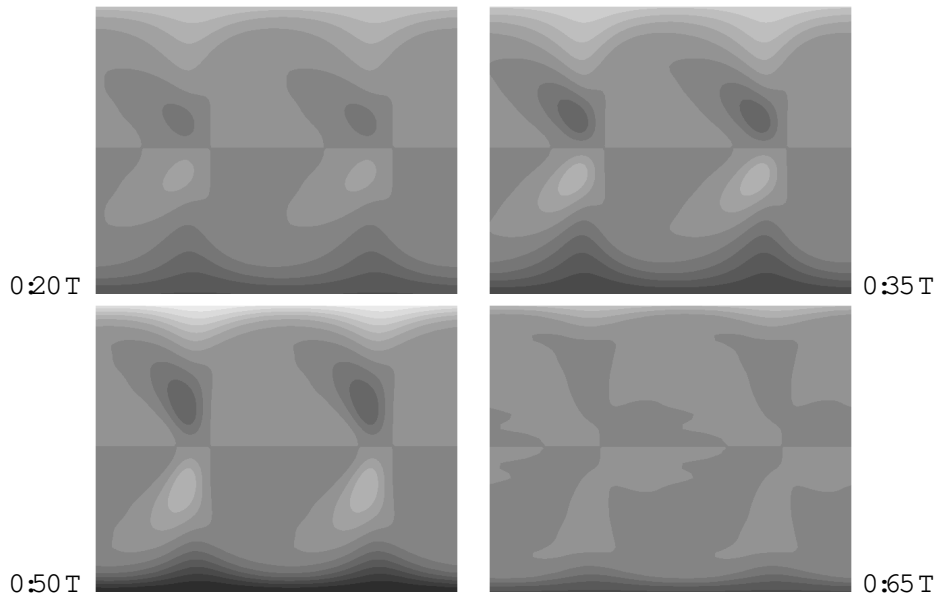


Figure 12: B_r at the surface during the failed reversal in Fig. 10. Reversed flux patches have insufficient time to migrate polewards before dissipating.